The American Journal of Pathology, Vol. 172, No. 2, February 2008

DOI: 10.2353/ajpath.2008.070076

Vascular Biology, Atherosclerosis and Endothelium Biology

Phosphorylation of Claudin-5 and Occludin by Rho Kinase in Brain Endothelial Cells

Masaru Yamamoto,*† Servio H. Ramirez,*† Shinji Sato,*† Tomomi Kiyota,*† Ronald L. Cerny,§ Kozo Kaibuchi,¶ Yuri Persidsky,*†‡ and Tsuneya Ikezu*†

From the Departments of Pharmacology and Experimental Neuroscience, and Pathology and Microbiology,‡ and the Center for Neurovirology and Neurodegenerative Disorders,† University of Nebraska Medical Center, Omaha, Nebraska; the Department of Chemistry,§ University of Nebraska, Lincoln, Nebraska; and the Department of Cell Pharmacology,¶ Nagoya University Graduate School of Medicine, Nagoya, Japan*

Critical to the proper maintenance of blood-brain-barrier (BBB) integrity are the endothelial tight junctions (TJs). Posttranslational modifications of essential endothelial TJ proteins, occludin and claudin-5, contribute and possibly disrupt BBB integrity. Our previous work has shown that Rho kinase (RhoK) activation mediates occludin and claudin-5 phosphorylation resulting in diminished barrier tightness and enhanced monocyte migration across BBB in the setting of human immunodeficiency virus-1 encephalitis (HIVE). To determine whether RhoK can directly phosphorylate TJ proteins, we examined phosphorylation of cytoplasmic domains of recombinant claudin-5 and occludin by RhoK. We found that RhoK predominately phosphorylated two sites on occludin (T382 and S507) and one site on claudin-5 (T207). Specific anti-phosphopeptide antibodies were developed for these sites, allowing the detection of phosphorylated occludin at T382 and S507, and claudin-5 at T207 from full-length recombinant occludin and claudin-5 transiently expressed in COS-7 cells and mouse brain microvascular endothelial cells. Finally, these phosphospecific antibodies demonstrated enhanced staining of brain endothelial cells in the mouse model for HIVE and human HIVE brains featuring mononuclear cell infiltration across disrupted BBB. Our results demonstrated the direct phosphorylation of occludin and claudin-5 by RhoK at specific sites, which was increased in encephalitic brain tissue. These antibodies could be useful reagents for monitoring BBB dysfunction *in vivo*. *(Am J Pathol 2008, 172:521–533; DOI: 10.2353/ajpath.2008.070076)*

The blood-brain-barrier (BBB) is composed of specialized nonfenestrated brain microvascular endothelial cells (BMVECs) connected by tight junctions (TJs) in an impermeable monolayer devoid of transcellular pores.[1] TJs are composed of claudins and occludin (OCC, integral membrane proteins) and intracellular proteins, zonula occludens (ZO-1 to ZO-3).[2] OCC (65-kDa protein) is highly expressed in BMVECs, and it is consistently found along the cell borders of brain endothelium.[3,4] OCC is composed of four transmembranous domains with the carboxyl and amino terminals oriented to the cytoplasm and two extracellular loops (44 amino acids and 45 amino acids) spanning the intercellular cleft.[5] OCC content is much lower in endothelial cells outside of the central nervous system[6,7] suggesting its active role in BBB function. The phosphorylation state of OCC regulates its association with the cell membrane and barrier permeability, and multiple phosphorylation sites have been identified on OCC serine and threonine residues.[8–10] The cytoplasmic C-terminal domain provides the connection of OCC with the cytoskeleton via accessory proteins, ZO-1 and ZO-2.[11]

Up to 24 claudins (20- to 24-kDa proteins) sharing the high sequence homology in the first and fourth transmembranous domains and extracellular loops have been identified in mammals.[12] Contiguous staining for claudins is found along endothelial cell borders in and outside the central nervous system. BMVECs express predominantly claudin-3 and -5 (CLD5).[3,13] The homophilic and heterophilic interactions between the extracellular loops of clau-

Supported in part by the National Institutes of Health (research grants P01 NS043985, R01 AA015913, and R01 MH65151 to Y.P.; R01 MH072539 to T.I.; and National Center for Research Resources P20RR15635 to T.I. and R.L.C.).

M.Y. and S.H.R. contributed equally in this study.

Accepted for publication October 16, 2007.

Address reprint requests to Tsuneya Ikezu, M.D., Ph.D., 985880 Nebraska Medical Center, Omaha, NE 68198-5880. E-mail: tikezu@unmc.edu, Yuri Persidsky, M.D., Ph.D., 985215 Nebraska Medical Center, Omaha, NE 68198-5215. E-mail: ypersids@unmc.edu.

dins ensure tight contacts of the cell monolayers.[14] Although overexpression of claudins can induce cell aggregation and formation of TJ-like structures, OCC expression does not result in TJ formation.[15] Nitta and colleagues[13] demonstrated that CLD5 is a critical determinant of BBB permeability in mice. Thus, it appears that claudins form the primary makeup of the TJs, and OCC further enhances TJ tightness.

The Rho family of small dimeric G proteins (GTPases, RhoA, Rac, Cdc42) are regulatory molecules that provide a link between membrane receptors and actin cytoskeleton and contribute to the regulation of endothelial barrier function, transendothelial leukocyte migration, and inflammation.[16] Stimulation with proinflammatory cytokines or leukocyte binding to adhesion molecules on endothelial cells results in RhoA and Rac1 activation leading to increased leukocyte adhesion and opening of intercellular gaps that allow leukocyte extravasation.[17–19]

Previously, we demonstrated that interactions between human immunodeficiency virus (HIV)-1-infected monocytes and BMVECs leads to RhoA activation, phosphorylation of TJ proteins, and decreased tightness of the BBB.[20] Furthermore, significant BBB injury (documented by disruption of CLD5/OCC staining) was detected in human brain tissues affected by HIV-1 encephalitis (HIVE), and monocytes co-cultured with BMVECs led to OCC and CLD5 phosphorylation via activation of RhoA and its downstream effector RhoK.[20] Consequently, inhibition of RhoA and RhoK blocked monocyte migration, prevented TJ phosphorylation and BBB leakiness. However, it was not clear whether RhoK could phosphorylate TJ proteins directly, and if so, which phosphorylation sites are targeted. In this study using recombinant RhoK and the C-terminal domains of CLD5 and OCC, we demonstrate the direct phosphorylation of OCC and CLD5 by RhoK. Also, using phosphopeptide mapping, phosphorylated sites on these two TJ protein domains were characterized and phosphospecific antibodies generated. Lastly, application of these antibodies proved useful in detecting alterations to the brain endothelium of HIV-1 encephalitic mice.

Materials and Methods

Preparation of Recombinant Glutathione S-Transferase-RhoK Fusion Protein (GST-RhoK), Histidine-Tagged Cytoplasmic Domain of Occludin (OCC-CT), and Cytoplasmic Domain of Claudin-5 (CLD5-CT)

A baculovirus expression vector of GST-RhoK, containing the catalytic domain (6 to 553 amino acids) of RhoK, was cloned and kindly provided by Dr. Kozo Kaibuchi at Nagoya University, Nagoya, Japan. Fusion proteins from the construct were produced in SF9 insect cells, using the baculovirus expression system, and purified by glutathione-Sepharose 4B (Pharmacia/GE Health Care, Pittsburgh, PA) column as described earlier.[21] 6xHistidine-tagged OCC-CT encoding the cytoplasmic region (378 to 521 amino acids) of mouse OCC was generated by subcloning the corresponding cDNA fragment (kindly provided by Dr. Shoichiro Tsukita, Kyoto University, Kyoto, Japan) into the *Bam*HI-*Eco*RI sites of pET28a *Escherichia coli* expression vector (Novagen/EMD Bioscience, San Diego, CA), induced by 0.1 mmol/L isopropyl-β-D-thiogalactopyranoside (Sigma-Aldrich, St. Louis, MO) in BL21DE3 *E. coli* (Novagen), and purified on a Ni-NTA column (Novagen). The His-tag sequence of purified OCC-CT was cleaved by thrombin (Sigma), which was removed by dialysis of the sample using Slide-A-Lyzer (molecular weight cutoff of 3.5 kDa; Pierce Biotechnology, Inc., Rockford, IL). The purity of the OCC-CT and GST-RhoK was determined as >90% by sodium dodecyl sulfate-polyacrylamide gel electrophoresis (SDS-PAGE) and R-250 Coomassie brilliant blue staining. The cytoplasmic C terminus domain of mouse claudin-5 (CLD5-CT, amino acids 199 to 218: KYSAPRRPTANGDYDKKNYV) was prepared as purified synthetic peptide with 100% purity (Alpha Diagnostic International, San Antonio, TX).

Phosphorylation Assay

The kinase reaction of substrate with purified GST-RhoK was performed in 50 μl of reaction buffer (50 mmol/L Tris/HCl at pH 7.5, 2 mmol/L EGTA, 1 mmol/L EDTA, 5 mmol/L $MgCl_2$) containing 200 μmol/L [γ-^{32}P] ATP (5 μCi; Perkin Elmer, Wellesley, MA), 0.5 μg purified RhoK, and the indicated amount of bovine myosin light chain (MLC, Sigma), purified OCC-CT recombinant protein, or CLD5-CT peptide. After incubation at 30°C, the reaction mixtures for MLC and OCC-CT were boiled in Laemmli sampling buffer[22] and subjected to SDS-PAGE. The radiolabeled bands were visualized and quantified by a phosphoimager (Typhoon System; Amersham Pharmacia Biotech, Arlington Heights, IL). For CLD5 peptides, the reaction mixtures were boiled and spotted onto phosphocellulose membrane (P81; Whitman, Maidstone, UK). The spots were excised and radioactivity levels were measured by liquid scintillation counter (Beckman Coulter, Inc., Fullerton, CA).

Liquid Chromatography/Tandem Mass Spectrometry (LC/MS/MS)

OCC-CT and CLD5-CT were phosphorylated by incubation with GST-RhoK in reaction buffer (50 mmol/L Tris/HCl at pH 7.5, 2 mmol/L EGTA, 1 mmol/L EDTA, 5 mmol/L $MgCl_2$, 200 μmol/L ATP) at 30°C for 20 hours. The samples were separated by SDS-PAGE and the stained bands were excised and subjected to LC/MS/MS analysis as described.[23] Briefly, in-gel trypsin digestion was performed (Promega, Madison, WI), and the digested peptides were extracted in 5% formic acid/50% acetonitrile and separated using a C18 reversed phase LC column (Dionex, Sunnyvale, CA).

A quadrupole-time of flight (Q-TOF) Ultima tandem mass spectrometer (Waters, Milford, MA) with electrospray ionization was used to analyze the eluting peptides.

The system was user-controlled using the MassLynx software v3.5 (Waters) in data-dependent acquisition mode with a 1-second survey scan (380 to 1900 Da) followed by up to three 2.4-second MS/MS acquisitions (60 to 1900 Da). The instrument was operated at a mass resolution of 8000 and was calibrated using the fragment ion masses of doubly protonated Glu-fibrinopeptides.

Database searches of the acquired MS/MS spectra were performed using Mascot (v1.9.0; Matrix Science, Boston, MA). The database was restricted to mouse proteins. The search parameters were as follows: no restrictions on protein molecular weight or pI, enzymatic specificity was set to trypsin, and phosphorylation was allowed as a variable peptide modification. Only peptides that gave a Mascot score greater than 13 ($P < 0.05$) for phosphorylated forms were considered as positive identifications.

Determination of Phosphorylation Sites of OCC-CT and CLD5-CT by RhoK by Synthetic Peptides

Because LC/MS/MS was unable to sequence lysine- or arginine-rich sequence after tryptic digestion of proteins, the following peptides were synthesized to examine their phosphorylation by GST-RhoK: KRAPTKGKAG (peptide 1, OCC 378-387), KQLKSKLAHIK (peptide 2, OCC 500-510 with S507A mutation), KQLKAKLSHIK (peptide 3, OCC 500-510 with S504A mutation), KYSAPRRPAA (peptide 4, CLD5 199-208 with T207A mutation), and KYSAPRRPTANGDYDKKNYV (peptide 5, CLD5 199-208). The phosphorylation assay for these peptides was performed as described.

Production of Phosphopeptide Antibodies for OCC and CLD5

Rabbits were immunized with phosphopeptides corresponding to OCC phospho-T382 [CKRAPT(PO_4)KGKAGKG], OCC phospho-S507 [CKQLKSKLS(PO_4)HIKRMV], or CLD5 phospho-T207 [CAPRRPT(PO_4)ANGDYDK] conjugated with keyhole limpet hemocyanin at their NH_2-terminal cysteine residue, followed by injection of complete Freund's adjuvant (Biosynthesis Inc., Lewisville, TX). After three boosts of antibody titer by peptide injection, antisera were preadsorbed three times with affinity column immobilized with corresponding nonphosphorylated synthetic peptide to remove nonspecific anti-peptide antibodies in the sera, followed by affinity purification using phosphopeptide column. The working dilutions of affinity-purified phosphopeptide antibodies were optimized using immuno-dot-blotting of synthetic phospho- and nonphosphopeptides.

Transfection, Immunoprecipitation, and Western Blotting

COS-7 cells were plated at 3×10^6 cells in 10-cm culture dishes and maintained in Dulbecco's modified Eagle's medium containing 10% fetal bovine serum. Constructs expressing either mouse OCC or CLD5 cDNA (cloned in pCDNA3.1$^+$; Invitrogen, Carlsbad, CA) were then transfected into COS-7 using LipofectAmine 2000 (Invitrogen). After 24 hours after transfection, cells were rinsed and treated (as indicated) for 24 hours with media containing the RhoK inhibitor, Y27632 (Calbiochem, La Jolla, CA). After incubation cells were rinsed twice with phosphate-buffered saline (PBS) and scraped in radioimmunoprecipitation assay (RIPA) buffer containing a broad specificity protease inhibitor cocktail (1:500 dilution, Sigma). Lysates were then triturated using a 21-gauge needle and centrifuged at $10,000 \times g$ for 5 minutes at 4°C. Protein concentration was then determined by bicinchoninic acid protein assay (Pierce), and 400 μg of total protein from each condition was used for immunoprecipitation. Immunoprecipitation was performed using protein A/G Plus-agarose beads (Santa Cruz Biotechnology, Santa Cruz, CA) following the manufacturer's recommendations. Briefly, the lysates were immunoprecipitated with commercial antibodies to OCC-1 (20 μg, Invitrogen) and CLD5 (20 μg; US Biologicals, Swampscott, MA) and subsequently precipitated with protein A/G agarose beads at 4°C overnight. Samples were rinsed several times with RIPA buffer and then boiled in 40 μl of SDS sample buffer for 5 minutes. Samples were loaded and resolved on SDS-PAGE (4 to 20% gradient gels, Pierce) and blotted to 0.2 μm nitrocellulose membranes (Amersham). Membranes were then probed with the commercial antibodies (described above) or the following generated phosphospecific antibodies: OCC (pT382, 1:500) and CLD5 (pT207, 1:500). Bound primary antibodies were detected with horseradish peroxidase-linked sheep anti-mouse or rabbit secondary antibodies (Abs) (1:15,000, Pierce), followed by addition of Supersignal West Pico chemiluminescent substrate (Pierce). Subsequent signal visualization was performed using the gel documentation system, G:Box Chemi HR16 (Syngene, Frederick, MD).

Transendothelial Electrical Resistance (TEER)

TEER was measured in real-time using the ECIS system (model 1600R; Applied Biophysics, Inc., Troy, NY), which was specifically designed to measure true barrier function, including resistance and capacitance. We used bEnd3 endothelial cell line (obtained from the American Type Tissue Collection, Manassas, VA) possessing functional characteristics of BMVECs (TJs, transporters, formation of tight monolayers, and response to astrocytic factors).[24,25] bEnd3 cells were grown to confluence on collagen type I-coated ECIS cultureware arrays (model 8W10E; Applied Biophysics, Inc.). Then, measurements were recorded with the following settings: current (1-volt), frequency (400 Hz), at 3-minute intervals. Both data acquisition and processing were performed using the ECIS data analysis software supplied by Applied Biophysics. The tightness of the endothelial barrier was indicated by TEER readings (typically $\sim$2600 Ω/cm^2). Treatments were performed as indi-

cated in the figure legends, and the data were represented as normalized resistance, which is the resistance measured after treatment over the resistance acquired before treatment introduction.

Human Peripheral Blood Lymphocytes in Nonobese Diabetic Severe Combined Immune-Deficient (Hu-PBL NOD/SCID) Mouse Model of HIVE

Monocytes and peripheral blood lymphocytes (PBLs) were obtained by countercurrent centrifugal elutriation of leukopheresis packs from HIV-1-, HIV-2-, and hepatitis B-seronegative donors.[26] Monocytes were cultured in suspension using Teflon flasks in Dulbecco's modified Eagle's medium (Sigma) supplemented with 10% heat-inactivated pooled human serum, 1% glutamine, 50 μg/ml gentamicin, 10 μg/ml ciprofloxacin (Sigma). If necessary, 1000 U/ml highly purified recombinant human macrophage colony-stimulating factor was added to the cultures for differentiation into monocyte-derived macrophages (MDMs). MDMs (after 7 days in culture) were infected for 18 hours with macrophage-tropic strain HIV-1_{ADA} at multiplicity of infection of 0.1.[26] The SCID mice (male NOD/C.B-17scid, 4 weeks old) were purchased from the Jackson Laboratory (Bar Harbor, ME). Animals were maintained in sterile microisolator cages under pathogen-free conditions in the Laboratory of Animal Medicine at the University of Nebraska Medical Center in accordance with ethical guidelines for care of laboratory animals set forth by the National Institutes of Health. Animals were injected intraperitoneally with rat anti-CD122 (0.25 mg/mouse) 3 days before PBL transplantation and twice with rabbit asialo-GM1 antibodies (0.2 mg/mouse) (Wako, Richmond, VA) 1 day before and 3 days after PBL injection (2×10^7 cells/mouse). HIV-1_{ADA}-infected MDMs (5 μl of suspension containing 3×10^5 HIV-infected cells) were injected intracerebrally[27] 8 days after PBL reconstitution generating hu-PBL-NOD/SCID HIVE mice.[28] Animals were sacrificed at 7, 14, and 21 days after inoculation.

Histopathology

Brain tissues collected at necropsy were snap-frozen in precooled isopentane or fixed in 4% phosphate-buffered paraformaldehyde and paraffin-embedded. Immunohistochemistry was performed on 10-μm frozen or 5-μm paraffin sections. The following Abs were used to detect total OCC and CLD5 (TJs, 1:50; Zymed, South San Francisco, CA), phosphorylated forms of OCC/CLD5 (using novel antibodies described in this report), vimentin (all human leukocytes, 1:50; DAKO, Carpinteria, CA), CD4/CD8 (human lymphocytes, 1:25; DAKO), CD68 (human MDM, 1:100; DAKO), vWF (BMVECs, 1:100; DAKO) (data not shown), glial fibrillary acid protein (astrocytes, 1:100; DAKO), Iba1 (microglia, 1:500; Wako Corp., Osaka, Japan), HIV-1 p24 antigen (1:10, DAKO).[28,29] Mouse neurons were labeled with mAbs for the neurofilament (NF, 1:100; DAKO).[30] For immunofluorescence, Alexa fluor-594-conjugated secondary Abs (at 1:400 dilution, Invitrogen) were introduced to the tissue sections at room temperature for 1 hour. After four rinses with PBS, the cells were analyzed under fluorescence microscopy using an epifluorescence Eclipse 80i microscope (Nikon, Tokyo, Japan), fitted with a CoolSnap-EZ digital camera (Photometrics, Tucson, AZ). Image acquisition/analysis was performed with Image-Pro (Media Cybernetics, Silver Spring, MD).

Table 1. Semiquantitative Assessment of Levels of TJ Protein Immunoreactivity Performed (n = 5 Serial Sections) Utilizing a Scale System Ranging from 0 to 3

	Control SCID (n = 3)	HIVE SCID (n = 7)	Control human cases (n = 2)	HIVE human cases (n = 4)
CLD5-pT207	0	3	0.5	3
OCC-pT382	0	1	N/A	N/A
OCC-pS507	0	2	1	3
Total CLD5	3	1.5*	3	1*
Total OCC	3	1*	3	1*

Scores of 0 = no positive staining in five ×20 fields (1.0 mm^2 each); 1 = weak staining in less than 25% of microvessels; 2 = strong staining in 30 to 60% of microvessels; 3 = strong staining in more than 70% of microvessels.

*Fragmented staining for TJ proteins was seen in HIVE human cases and HIVE mice.

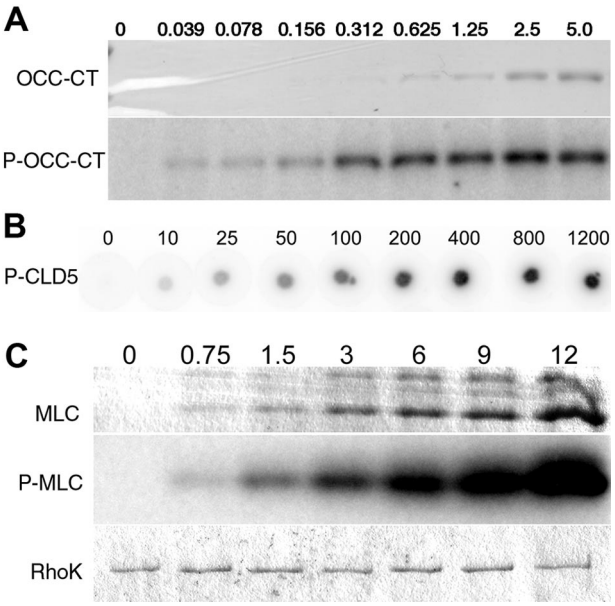

Figure 1. Dose-dependent analysis of phosphorylation of CLD5-CT peptide, MLC, and OCC-CT by GST-RhoK. **A** and **C:** Increasing doses of OCC-CT (0 to 5 μmol/L, **A**) or MLC (0 to 12 μmol/L, **C**) were incubated with [γ-^{32}P] ATP and purified GST-RhoK and separated on SDS-PAGE, followed by R-250 Coomassie brilliant blue staining (CBB, **top**) and autoradiogram (**middle**) of OCC-CT (**A**) or MLC (**C**). **B:** Increasing doses of CLD5-CT (0 to 1200 μmol/L, **B**) or were phosphorylated by GST-RhoK, and spotted onto phosphocellulose membrane. After extensive washing, the $^{32}PO_4$ incorporation was visualized by Typhoon Phosphoimager. **C: Bottom** shows the CBB-stained GST-RhoK on the same gel.

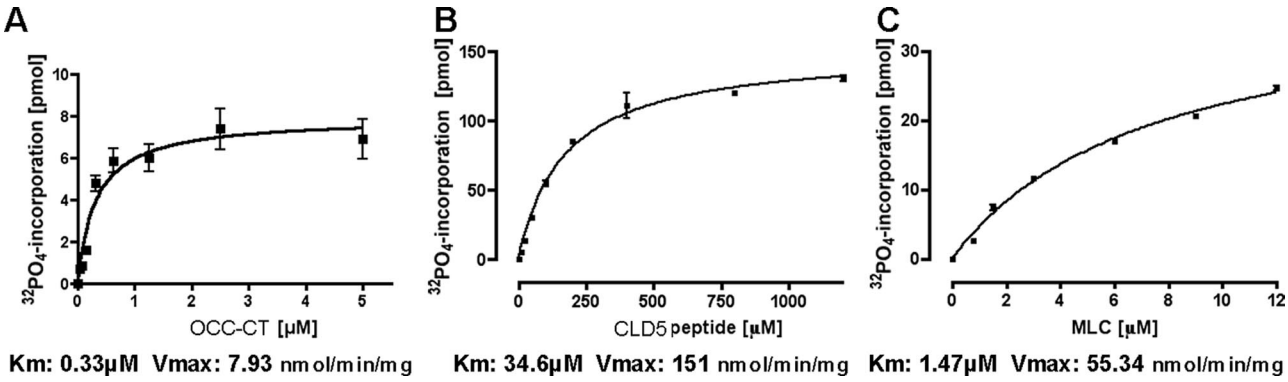

Figure 2. Kinetics of substrate phosphorylation by GST-RhoK. Dose response curves of OCC-CT (**A**), CLD5-CT (**B**), and MLC (**C**). K_m and V_{max} values were presented as μmol/L and nmol/minute/mg, respectively, from the complied data of three independent experiments.

Human Brain Tissue

Frontal cortex specimens derived from four HIVE cases of different severity (two severe and two moderate according to previously described criteria[20]) and two seronegative age-matched controls were provided by the National NeuroAIDS Consortium (Washington, DC) (Table 1). Approval was obtained from the University of Nebraska Medical Center institutional review board for these studies. Serial frozen sections (5 μm thick) were cut and double immunostained (indirect immunofluorescence) for total OCC/HAM56 and CLD5/HAM56 or phospho-OCC (at S507 and T382) and phospho-CLD5 (at T207) as described.[20]

Assessment of Immunostaining

Semiquantitative assessment of immunostaining for OCC, CLD5, phospho-OCC (at S507 and T382), and phospho-CLD5 (at T207) was performed using five sections per brain, and three to seven brains per group.

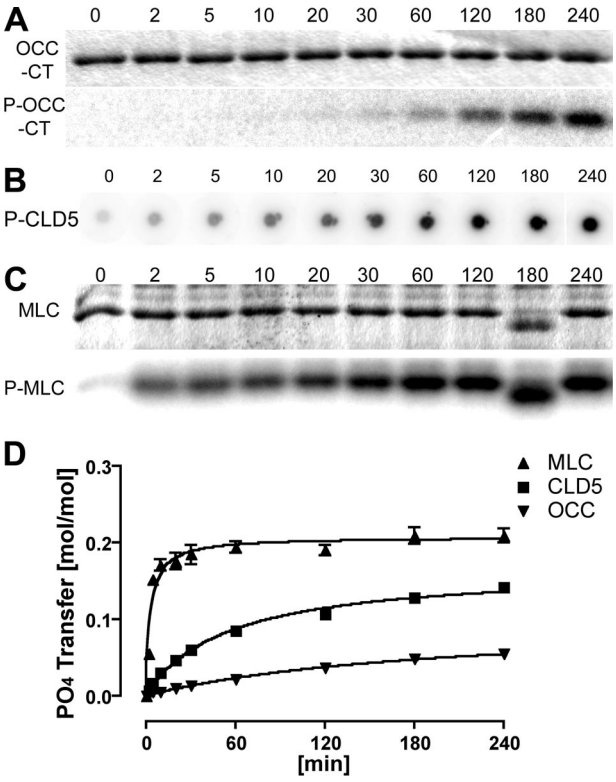

Figure 3. Time course of substrate phosphorylation by GST-RhoK. **A** and **C:** OCC-CT (5 μmol/L) or MLC (9 μmol/L, **C**) was incubated with 200 μmol/L [γ-^{32}P] ATP (10 μCi) and purified 1-μg GST-RhoK in 100-μl volume for 0 to 240 minutes, and a 10-μl aliquot was mixed with Laemmli sampling buffer and boiled for 5 minutes at each time point. The samples were subjected to SDS-PAGE for CBB staining (**top**) and autoradiogram (**bottom**). **B:** The same condition was applied to CLD5-CT peptide (800 μmol/L, **B**), and 10-μl aliquots were spotted onto phosphocellulose membrane for each time point. After extensive washing, the membrane was subjected to autoradiogram. **D:** The time course of substrate phosphorylation by quantification of autoradiogram compiled from three independent experiments. *y* axis represents the number of phosphates transferred to each substrate (mol/mol).

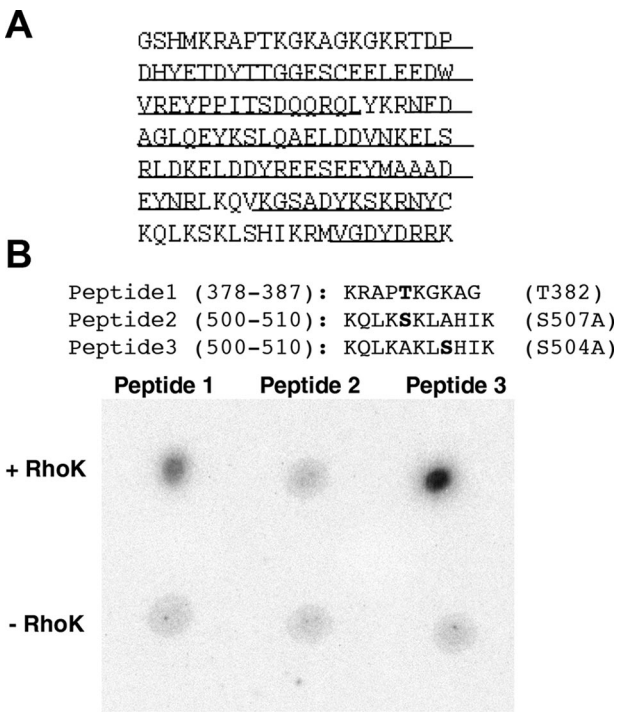

Figure 4. Phosphopeptide mapping of OCC-CT. **A:** Amino acid sequence of purified OCC-CT. The **underlined** portions were determined by LC/MS/MS. No significant phosphorylation sites were detected. **B:** Phosphorylation of synthetic peptides corresponding to mouse OCC 378-387 with T382 (peptide 1), 500-510 with S507A mutation (peptide 2), and 500-510 with S504A mutation (peptide 3) by purified GST-RhoK. The autoradiogram shows phosphorylation of peptides 1 and 3.

Staining results were blindly quantified by the following scoring system: 0 = no positive staining in five ×20 fields (1.0 mm^2 each); 1 = weak staining in less than 25% of microvessels; 2 = strong staining in 30 to 60% of microvessels; and 3 = strong staining in more than 70% of microvessels.

Results

We examined the phosphorylation of the cytoplasmic C-terminal domains of mouse OCC and CLD5 using recombinant OCC 378-521 protein (OCC-CT) and synthetic peptide corresponding to CLD5 199-218 (CLD5-CT) by catalytic domain of RhoK 6-553 (GST-RhoK) *in vitro* (Figure 1, A and B). Dose-dependent increase of substrate phosphorylation was observed in both OCC-CT (0 to 5 μmol/L, Figure 1A) and CLD5-CT (0 to 1200 μmol/L, Figure 1B). MLC (0 to 12 μmol/L, Figure 1C) was used as a control substrate of GST-RhoK.[21,31] GST-RhoK phosphorylated OCC-CT, CLD5-CT, and MLC with K_m of 0.33, 34.6, and 1.47 μmol/L and V_{max} of 7.93, 15.1, and 55.3 nmol/minute/mg, respectively (Figure 2, A–C). The time course of phosphorylation was also tested for the incubation of 0 to 240 minutes (Figure 3, A–D). The MLC phosphorylation reached plateau at 60 minutes (Figure 3, C and D), whereas the phosphorylation of OCC-CT (Figure 3, A and D) and CLD5-CT (Figure 3, B and D) was unsaturated up to 240 minutes. These data suggested that RhoK could directly phosphorylate CLD5-CT and OCC-CT; however, their phosphorylation kinetics were not as efficient as MLC.

Our previous work using human brain tissues with HIVE and *in vitro* BBB models (human BMVECs) indicated that interactions between HIV-1-infected or uninfected monocytes during their migration across the barrier 1) decrease its integrity, 2) lead to phosphorylation of TJ proteins via activation of RhoA and RhoK,[20] and 3) inhibition of RhoA/RhoK prevents monocyte migration, TJ phosphorylation, and barrier impairment. The results presented here suggest that persistent RhoK activation (as seen during monocyte infiltration during HIVE[20]) is necessary for OCC and CLD5 phosphorylation.

To determine the phosphorylation sites of OCC-CT by GST-RhoK, the phosphorylated OCC-CT protein was subjected to phosphopeptide mapping using LC/MS/MS with the system previously described.[32] As shown in Figure 4A, 107 amino acids of 148 residues (72%) were covered by LC/MS/MS and no phosphorylation sites were

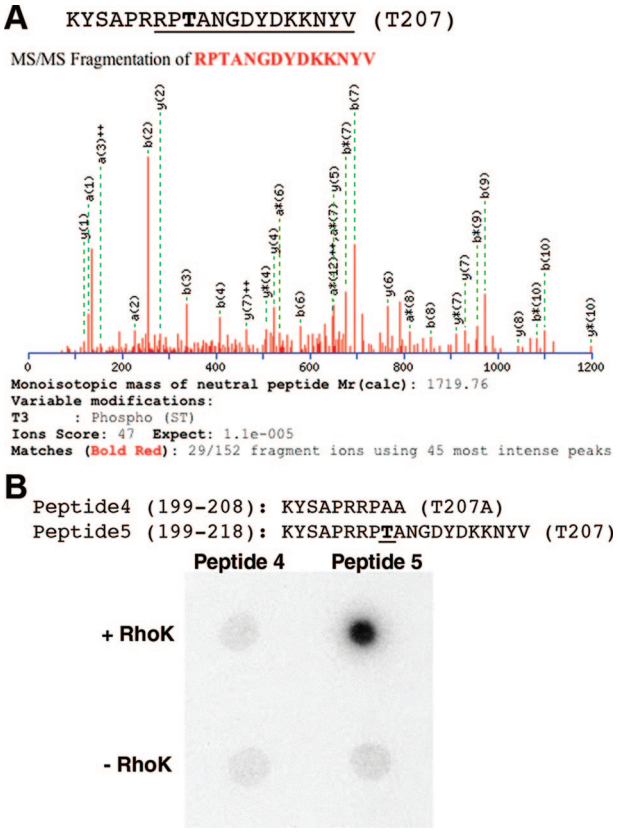

Figure 5. Phosphopeptide mapping of CLD5-CT peptide. **A:** Amino acid sequence of CLD5-CT peptide. The **underlined** portion was determined by LC/MS/MS. The phosphorylation site (T207) is in bold. MS/MS fragmentation of trypsin-digested peptide fragment (mouse CLD5 205-218) detected T207 phosphorylation (Ions score, 47; expectation, 1.1e-0.05). **B:** Phosphorylation of synthetic peptides corresponding to mouse clauding-5 199-208 (peptide 4), and 199-218 (peptide 5) by purified GST-RhoK. The autoradiogram shows phosphorylation of peptide 5.

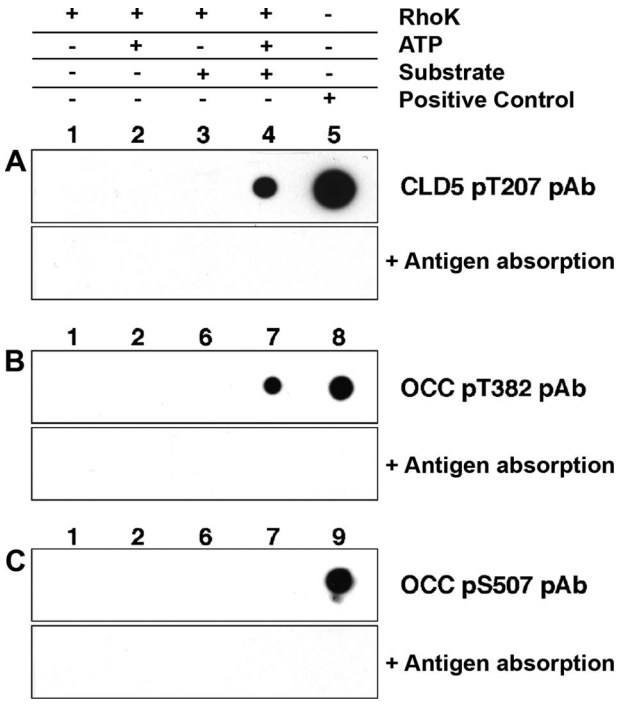

Figure 6. Detection of CLD5 and OCC phosphorylation by specific anti-phosphopeptide antibodies. **A–C: Top**: CLD5 cytoplasmic sequence peptide (**A**, 500 ng per spot) or OCC cytoplasmic protein fragment (**B** and **C**, 2 μg per spot) were incubated with GST-RhoK (200 ng/μl) overnight at 30°C, and spotted onto polyvinylidene difluoride membrane for dot-blotting using anti-CLD5 pT207 (**A**), anti-OCC pT382 (**B**), or anti-OCC pS507 antibody (**C**). Each antibody was preincubated with 10 μg/ml of corresponding antigen phosphopeptide before the immunoblotting for antigen absorption (**bottom**, **A–C**). **Lane 1**, Two hundred ng of RhoK without ATP; **lane 2**, 200 ng of RhoK with 1 mmol/L ATP; **lane 3**, 500 ng of CLD5 peptide with 200 ng of RhoK without ATP; **lane 4**, 500 ng of CLD5 peptide with 200 ng of RhoK and 1 mmol/L ATP; **lane 5**, 500 ng of CLD5 pT207 phosphopeptide; **lane 6**, 2 μg of OCC-CT with 200 ng of RhoK without ATP; **lane 7**, 2 μg of OCC-CT with 200 ng of RhoK and 1 mmol/L ATP; **lane 8**, 500 ng of OCC pT382 phosphopeptide; **lane 9**, 500 ng of OCC pS507 phosphopeptide.

detected. To examine the uncovered sequences, we synthesized corresponding peptides (peptide 1, 378-387; peptide 2/3, 500-510), which contained one potential phosphorylation site per peptide sequence (Figure 2B). To distinguish the phosphorylation of S504 and S507, either site was mutated to alanine (A) in peptides 2 and 3. GST-RhoK phosphorylated peptides 1 and 3 (Figure 4B). These data suggested that RhoK phosphorylated OCC at T382 and S507.

To determine the phosphorylation of CLD5-CT, the phosphorylated peptide was also analyzed by LC/MS/MS, which detected phosphorylation of T207 (Figure 5A). Because LC/MS/MS could not cover amino acids 199 to 204, the phosphorylation of S201 was determined by generating synthetic peptides (peptide 4, 199 to 208; and peptide 5,199 to 218). In peptide 4, T207 was mutated to alanine (A) to distinguish phosphorylation of S201 and T207 (Figure 5B). GST-RhoK phosphorylated peptide 5 but not 4 (Figure 5B). Our results indicated that RhoK phosphorylated CLD5 at T207.

To further characterize TJ phosphorylation, we generated and affinity-purified anti-phospho-OCC and phospho-CLD5 antibodies using three synthetic phosphopeptides against the determined sequences. These affinity-purified antibodies showed specificity to the target phosphoresidues without cross reactivity to nonphosphorylated peptides of the same sequence or other phosphopeptides of different sequences (data not shown). Using these antibodies, we examined if the cytoplasmic region of OCC and CLD5 were phosphorylated by GST-RhoK at the specific phosphorylation sites. The phosphorylation

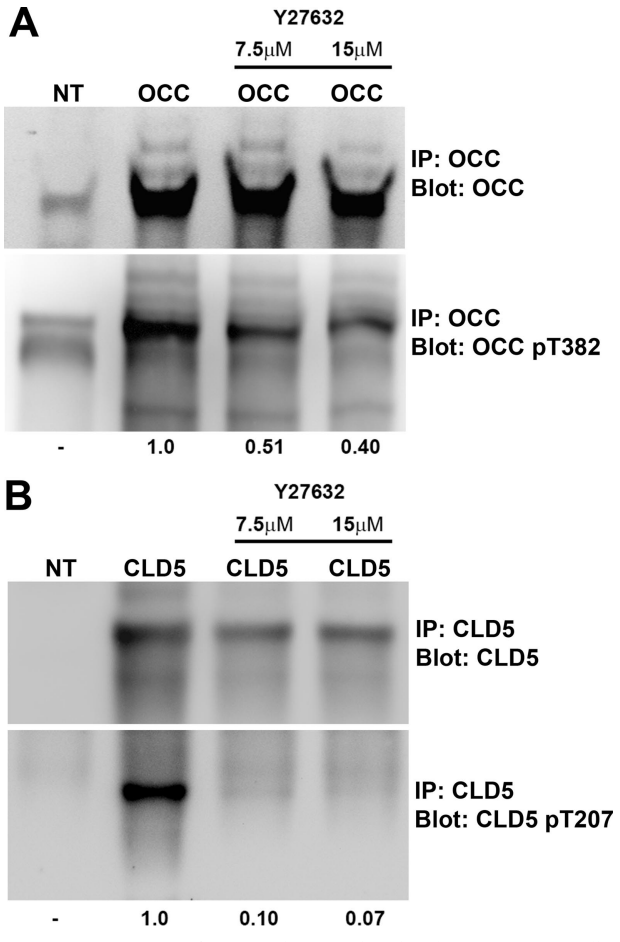

Figure 7. Detection of OCC and CLD5 phosphorylation in COS-7 cells. COS-7 cells were transfected with full-length wild-type mouse OCC or CLD5 mammalian expression vector, and treated or untreated with RhoK inhibitor Y27632 (7.5 or 15 μmol/L) for 16 hours. The plasma membrane samples were lysed in 1% Trion X-100 and subjected to immunoprecipitation using 20 μg of anti-OCC (**A**), or CLD5 mouse monoclonal antibodies (**B**) plus protein A/G Plus-Sepharose. Immunoblotting for OCC and p-OCC (pT382, **A**) or CLD5 and p-CLD5 (pT207, **B**) was performed on immunoprecipitated samples using specific rabbit polyclonal antibodies. IP and blot (**A** and **B**) indicate specific molecules for immunoprecipitation and immunoblotting, respectively. **A** and B: NT; no transfection; OCC, transfected recombinant mouse OCC; Cld-5, recombinant mouse CLD5. The number at the **bottom** indicates changes in arbitrary unit of the immunoreactive band intensity of p-OCC (pT382, **A**) or p-CLD5 (pT207, **B**) after Y27632 treatment.

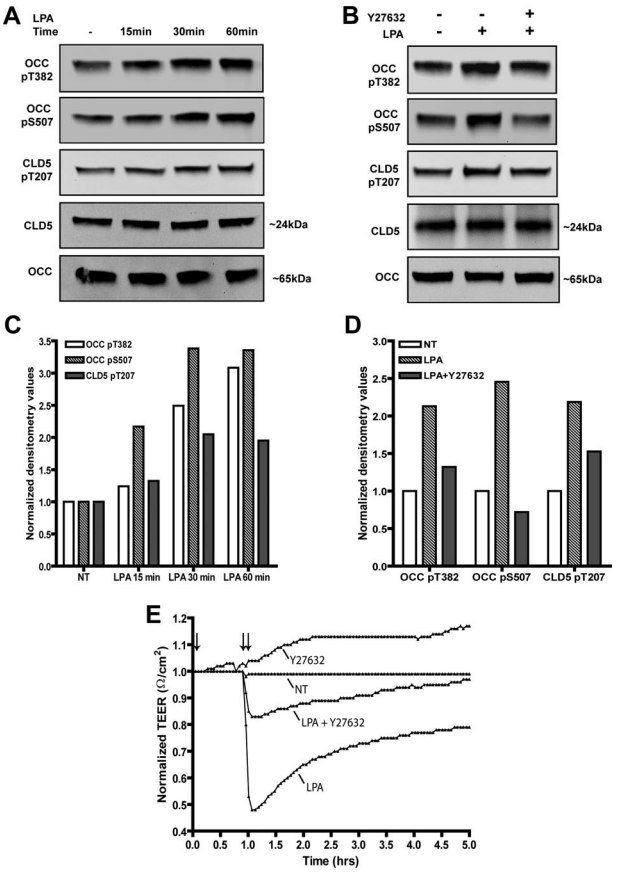

Figure 8. Detection of LPA-induced OCC and CLD5 phosphorylation and TEER reduction in mouse BMVECs. Western blots were performed using novel phosphospecific antibodies, OCC pT382, OCC pS507, and CLD5 pT207 in mouse brain endothelial cells; nonphoshospecific antibodies recognizing total OCC and total claudin5 are also indicated. **A** and **C:** Cells were cultured under reduced serum conditions (1% FBS) for 24 hours and then stimulated with 10 μmol/L LPA for the indicated time points; or **B** and **D:** pretreated with 2 μmol/L Y27632 for 1 hour followed by stimulation with 10 μmol/L LPA for 30 minutes. Corresponding densitometry analysis of the Western blots is shown below (**C**, **D**), the densitometry values represent the ratio of phosphorylated to unphosphorylated as compared with the nontreated (NT) condition. **E:** Endothelial cell monolayers were formed on ECIS electrode culture slides (described in Materials and Methods) and real time measurements of TEER were acquired. The measurements shown represent recordings acquired at 3-minute intervals at the parameters described in the Materials and Methods. The **single arrow** designates the pretreatment (1 hour) with 2 μmol/L of Y27632 with or without co-incubation of 10 μmol/L LPA as shown by the **double arrow**. The data are presented as normalized resistance for each condition, which is the resistance measured after treatment over the resistance acquired before treatment introduction (typically ~2600 Ω/cm^2). Representative data of three independent experiments are shown.

of T207 of CLD5-CT and T382 of OCC-CT was detected by respective specific antibody (Figure 6, A and B; lane 4). Phosphorylation of S507 of OCC-CT was undetectable, whereas positive control (phosphopeptide for pS507; Figure 6C, lane 9) was identified by the specific antibody. These data suggested that RhoK phosphorylated CLD5-CT at T207 and OCC-CT at T382, whereas S507 of OCC-CT was minimally phosphorylated by RhoK.

Using these antibodies, we tested whether specific residues were phosphorylated in cultured cells. Full-

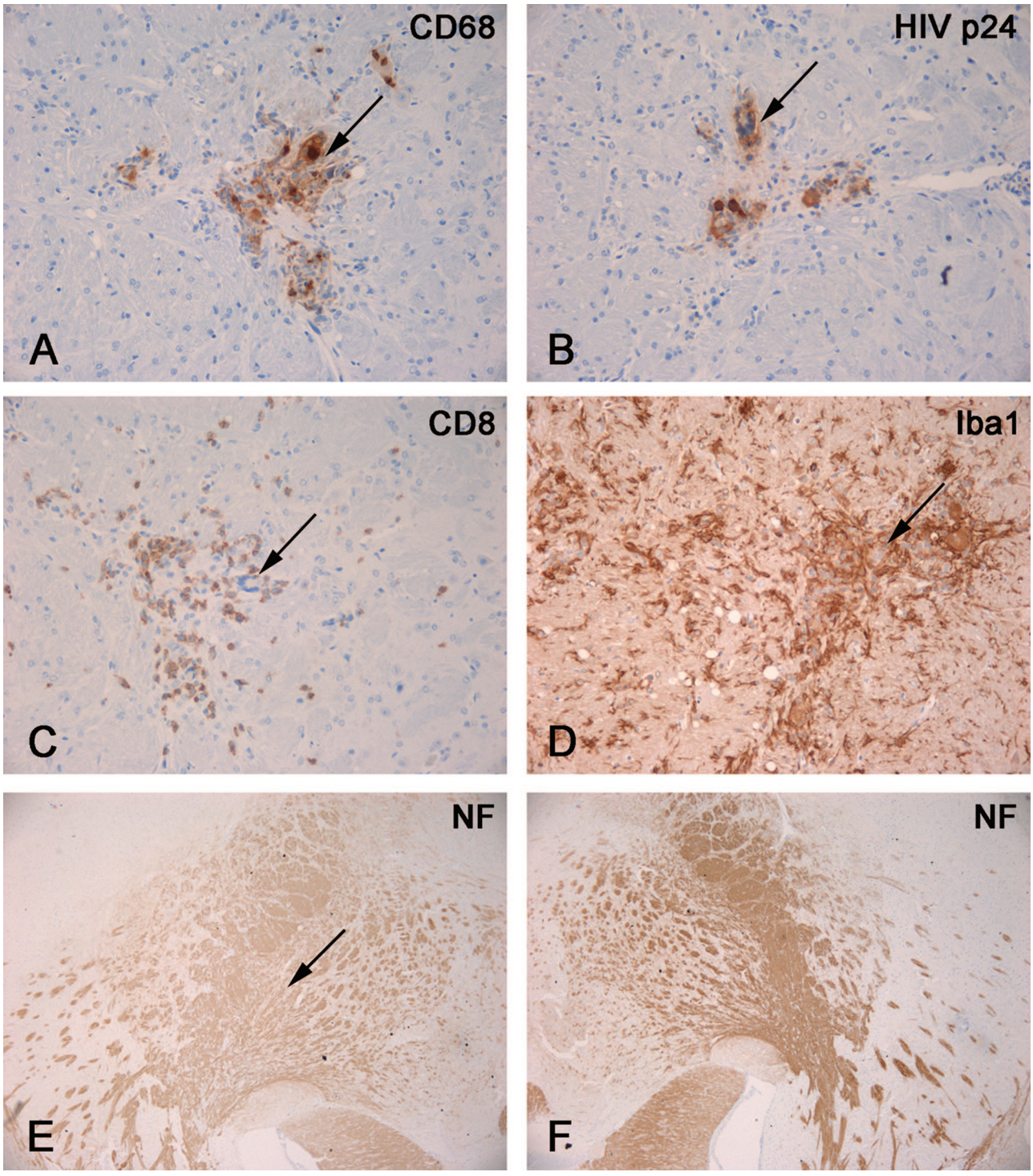

Figure 9. Neuropathological features of HIVE in hu-PBL-NOD/SCID HIVE mice. Mice were reconstituted with human PBL and sacrificed 2 weeks after injection of HIV-1-infected MDM in brains. Serial mouse brain sections stained with antibodies to human CD68 (**A**), HIV-p24 (**B**), human CD8 (**C**), Iba1 (**D**), or NF (**E**, **F**). Primary Abs were detected by Vectastain Elite kit with DAB as a substrate. **A** and **B:** $CD68^+$ human MDM (**arrow**, **A**) in the basal ganglia were HIV-1 $p24^+$ (**arrow**, **B**). **C:** $CD8^+$ lymphocyte infiltrated in the areas containing virus-infected macrophages (**arrow**). **D:** These areas featured prominent microglial reaction ($Iba1^+$, **arrow** indicates location of MDM). **E** and **F:** Decreased staining for neuronal marker (NF) was found in injected hemisphere (**arrow** indicates area of injection, **E**) as compared to contralateral (noninjected, **F**). Original magnifications: ×200 (**A–D**); ×40 (**E**, **F**).

length wild-type OCC and CLD5 were transiently expressed in COS-7 cells, and replicate cells were treated with RhoK inhibitor (Y27632). Cells were lysed, and the plasma membrane fraction was collected followed by immunoprecipitation and immunoblotting. We detected endogenous phosphorylated OCC (p-OCC) in COS-7 (Figure 7A, lane 1). Overexpression of recombinant OCC increased both total and phosphorylated p-OCC (Figure 7A, lane 2), and phosphorylation was reduced by RhoK inhibitor (Figure 7A, lanes 3 and 4). COS-7 cells had no endogenous CLD5 (Figure 7B, lane 1). Overexpression of recombinant CLD5 showed phosphorylation at T207 (p-CLD5; Figure 7B, lane 2), which was diminished by Y27632 treatment (Figure 7B, lanes 3 and 4). Thus, both OCC and CLD5 were phosphorylated at the specific residues. Whereas OCC phosphorylation is partly dependent on RhoK, CLD5 phosphorylation appears to be very specific for RhoK.

We have also examined whether OCC and CLD5 phosphorylation is associated with functionally impaired TJs. Confluent monolayers of mouse BMVECs (bEnd3 cell line, known to express TJ molecules, such as OCC and claudin-5, and widely used for BBB studies *in vitro*[24,25,33,34]) with established TJs were treated with lysophosphatidic acid (LPA), a known activator of RhoA[35] and inducer of BBB impairment. LPA-induced RhoA activation resulted in phosphorylation of OCC (at both S507 and T382) and CLD5 (at T207) (Figure 8, A and C). RhoA activation also led to reduced barrier tightness, as indicated by diminished TEER (Figure 8E). LPA-induced phosphorylation of OCC and CLD5 and reduction in TEER were prevented by RhoK inhibitor, Y27632 (Figure 8, B, D, and E), demonstrating RhoK-dependent signaling in brain endothelial cells. These data demonstrate direct association between OCC and CLD5 phosphorylation and functionally impaired TJs.

Finally, we examined the phosphorylation status of the TJ proteins in the well established animal model of HIVE (hu-PBL NOD/SCID HIVE mice) that reproduces a number of key features of human HIV-1 central nervous system infection.[36] Neuroinflammatory responses, neuronal dysfunction, mononuclear cell infiltration across the BBB, and BBB injury were reproduced in these animals.[28] The immune system of NOD/SCID mice was repopulated with human PBL, and 1 week after PBL reconstitution, HIVE was induced by stereotactic inoculation of autologous HIV-infected MDM into the basal ganglia (generating hu-PBL-NOD/SCID HIVE mice) (Figure 9, A and B). We previously demonstrated specific antiviral cellular responses in this model and presence of $CD8^+$ T lymphocytes in areas containing MDM in the brain.[28,29,36] The presence of virus-specific cytotoxic T lymphocytes (CTL) (Figure 9C) resulted in significant elimination of HIV-1 MDM as compared to control animals (injected with MDM intracerebrally without prior PBL transfer).[28,36,37] Astrogliosis and microglial reaction (Figure 9D) were evident in these animals, being proportional to the level of mononuclear cell infiltration. Brain tissue of hu-PBL-NOD/SCID HIVE mice showed neuronal injury (documented by decreased staining for NF; Figure 9, E and F) consistently seen in the areas of neuroinflammation, which paralleled neuronal and cognitive impairment as tested by hippocampal electrophysiology and water maze tests.[30] In addition, mice developed viremia because of infection of circulating $CD4^+$ lymphocytes.

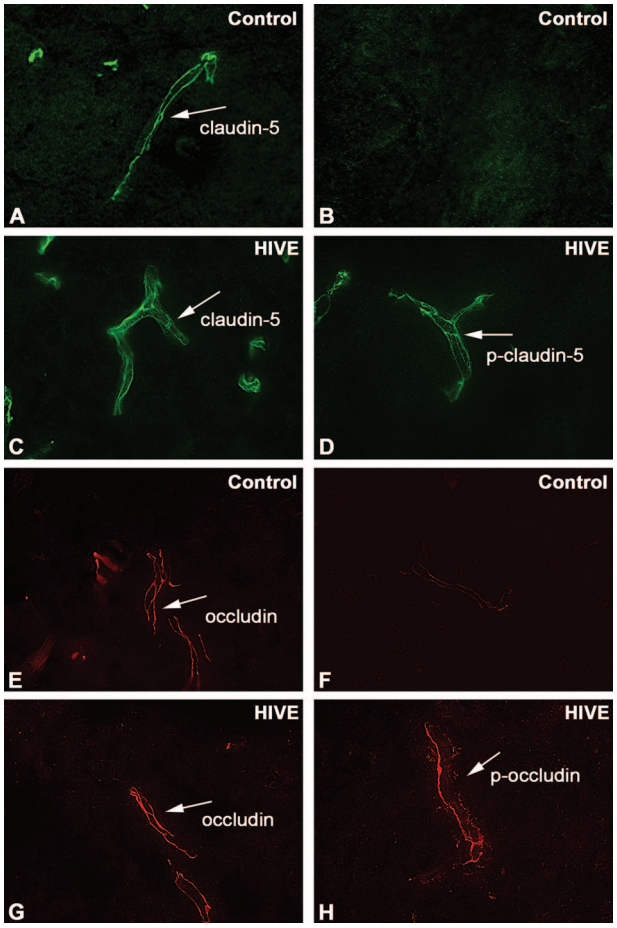

Figure 10. Detection of OCC and CLD5 phosphorylation in brain tissues of hu-PBL-NOD/SCID HIVE mice. **A–H:** Ten-μm-thick frozen sections of mouse brains were prepared at 14 days after sham injection (**A**, **B**, **E**, **F**) or intracerebral injection of HIV-1-infected MDM (**C**, **D**, **G**, **H**). The sections were stained with anti-CLD5 (**A**, **C**), anti-CLD5 pT207 (**B**, **D**), anti-OCC (**E**, **G**), or anti-OCC pT382 antibodies (**F**, **H**) and fluorescence-conjugated secondary antibodies. **A–H:** Oil immersion. Original magnifications, ×1000.

TJ proteins of BMVECs were immunohistochemically evaluated in animals intracerebrally injected with HIV-1-infected MDM (HIVE mice) and sham-treated mice (5 μl of media without MDM). We examined seven brains of mice with HIVE and three controls using antibodies to TJ proteins and p-OCC and p-CLD5. As shown in Figure 10, antibodies against total CLD5 and OCC stained brain endothelial cells in sham and HIVE mouse brains (Figure 10, A, C, E, and G). In contrast, assessment of TJs by phosphospecific CLD5 and OCC antibodies showed significant increase in staining of HIVE mice (Figure 10, D and H) as compared with sham-inoculated controls (Figure 10, E and F). Diminished staining of total OCC and CLD5 (Figure 11, A–D) and increased expression of phosphorylated TJ proteins (Figure 11, E–H) were found in areas of mononuclear cell infiltration as well as on some vessels without infiltration. These findings suggest that other factors (such as proinflammatory molecules

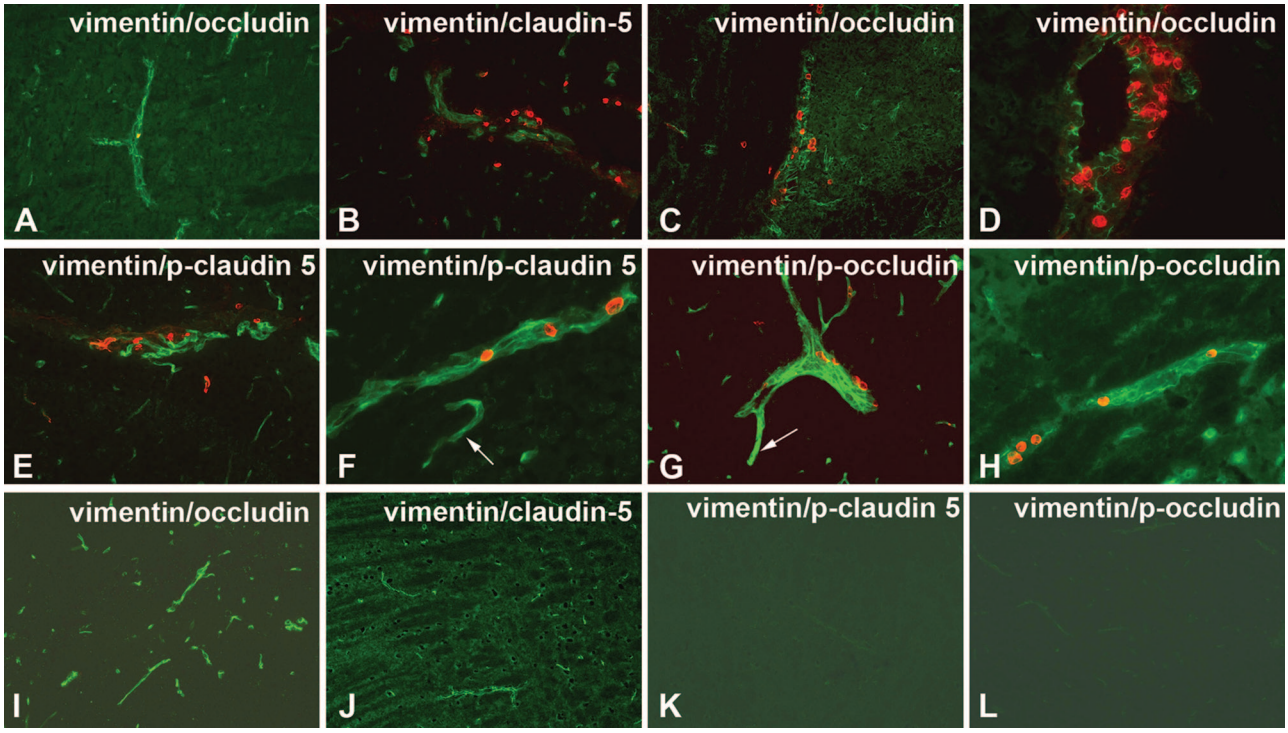

Figure 11. Expression of phosphorylated TJ proteins correlated with mononuclear cell infiltration in hu-PBL-NOD/SCID HIVE mice. Ten-μm-thick frozen sections of mouse brains were prepared at 14 days after intracerebral injection of HIV-1-infected MDM (**A–H**) or control mice (**I–L**). The sections were double immunostained with anti-vimentin and anti-OCC (**A**, **C**, **D**, **I**), CLD5 (**B**, **J**), anti-CLD5 pT207 (**E**, **F**, **K**), or anti-OCC pS507 antibodies (**G**, **H**, **L**) and fluorescence-conjugated secondary antibodies. Whereas TJs were well preserved in areas without mononuclear cell infiltrate (**A**), both CLD5 (**B**) and OCC (**C**, **D**) showed fragmented staining in areas containing inflammatory cells (red, vimentin). Antibodies to p-CLD5 (pT207, **E** and **F**) and p-OCC (pS507, **G** and **H**) highlighted microvessels featuring migration or perivascular accumulation of mononuclear cells (red). Brain endothelium outside of areas featuring inflammatory infiltrate also featured positive staining with p-OCC or p-CLD5 (**arrow**), albeit less intensive (**E** and **G**) in HIVE mice. Control animals demonstrated contiguous TJ immunostaining (OCC, I; and CLD5; **J**), whereas phosphospecific antibodies to TJ proteins produced no staining (**K**, **L**). Fluorescence-conjugated. Original magnifications: ×200 (**A–C**, **E**, **G**, **I–L**); ×400 (**D**, **F**, **H**).

and viral proteins) could lead to BBB impairment. Although contiguous OCC and CLD5 were easily detected in control mice (Figure 11, I and J), antibodies to p-OCC or p-CLD5 produced no staining (Figure 11, K and L). Semiquantitative assessment of immunostaining with phosphospecific antibodies indicated low score in control as compared to HIVE mice (Table 1).

We also tested antibodies to phosphorylated TJ proteins in human brain tissues (four HIVE and two seronegative controls). As expected, CLD5 and OCC (Figure 12, A and D) showed fragmented staining in areas containing monocyte/macrophage infiltrate. Antibodies to p-CLD5 and p-OCC highlighted microvessels in brain tissues affected by HIVE (Figure 12, B, C, E, and F). Control brains demonstrated contiguous CLD5 immunostaining and few perivascular macrophages (Figure 12G), whereas phosphospecific antibodies to TJ proteins produced no staining (Figure 12, H and I). Blind semiquantitative evaluation of immunostaining with phosphospecific antibodies demonstrated lower scores in controls as compared to HIVE cases (Table 1). These data suggest that TJ phosphorylation was enhanced in HIVE paralleling BBB injury and mononuclear cell infiltration. Thus, these antibodies could be used as markers of BBB instability and RhoK-mediated phosphorylation.

Discussion

Accumulating evidence suggests the role of RhoK in the regulation of BBB integrity via modification of TJ proteins ensuring barrier tightness.[38] Our previous results pointed to RhoK as a potential kinase of TJ proteins, activation of which might be the molecular mechanism mediating BBB dysfunction in neuroinflammation.[20] This study demonstrated that RhoK indeed phosphorylated cytoplasmic domains in CLD5 and OCC at specific sites. Using mouse BMVECs we demonstrated OCC and CLD5 phosphorylation at all three specific sites after RhoA/RhoK activation, and these changes were accompanied by functional impairment of the barrier and were prevented by specific RhoK inhibitor. Furthermore, we detected phosphorylation of TJ proteins by RhoK at the same sites using an *in vitro* cellular system and HIVE model *in vivo*. Although OCC phosphorylation was shown to be associated with loosening of BBB in functional assays,[39] its phosphorylation sites were not thoroughly investigated. Andreeva and colleagues[40] demonstrated that protein kinase C (PKC) could phosphorylate OCC at S338 leading to its translocation to the cell-cell contacts. Casein kinase 2 (CK2) phosphorylated OCC at T375 and S379,[41] and *in vitro* studies pointed to CK2 as OCC kinase.[42] However, the paucity of the phosphorylation

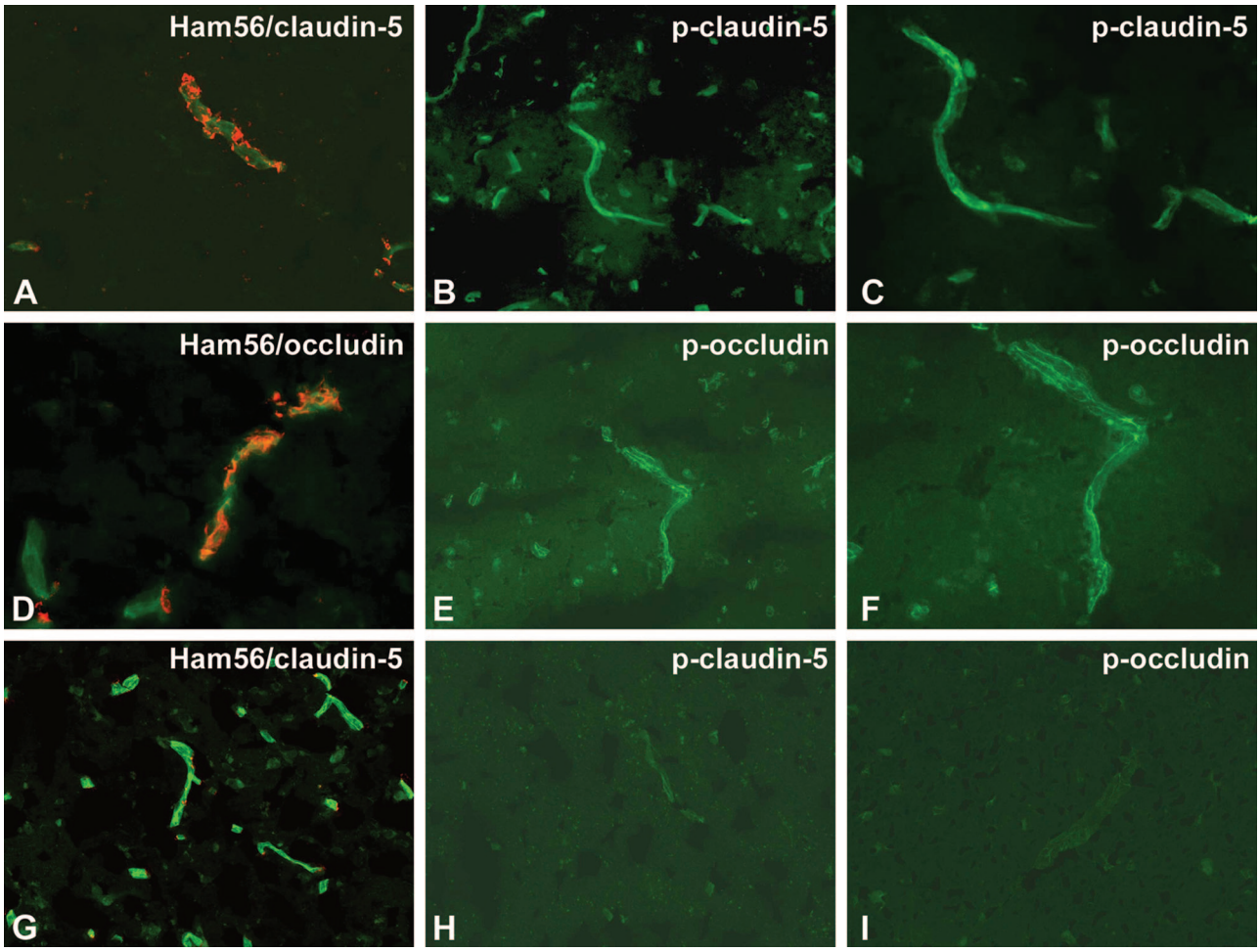

Figure 12. Expression of phosphorylated TJ proteins in human brain tissues with HIVE. Ten-μm-thick frozen sections of human brains with HIVE (**A–F**) or controls (**G–I**) were cut. The sections were double immunostained with Ham56 (macrophage marker) and anti-CLD5 (**A**, **G**) or OCC (**D**), anti-CLD5 pT207 (**B**, **C**, **H**), or anti-OCC pS507 antibodies (**E**, **F**, **I**) and fluorescence-conjugated secondary antibodies. CLD5 (green, **A**) and OCC (green, **D**) showed fragmented staining in areas containing inflammatory cells (red, Ham56 monocyte/macrophage marker). Antibodies to p-CLD5 (pT207, **B** and **C**) and p-OCC (pS507, **E** and **F**) highlighted microvessels (**arrows**). Control brains demonstrated contiguous CLD5 immunostaining (green) and few perivascular monocytes/macrophages (red) (CLD5, **G**), whereas phosphospecific antibodies to TJ proteins produced no staining (OCC pS507, **H**; CLD5 pT207, **I**). Original magnifications: ×200 (**A**, **B**, **D**, **E**, **G**, **H**, **I**); ×400 (**C**, **F**).

sites by PKC contrasted with the multiple phosphorylation residues found in previous reports[8] suggesting the involvement of other kinases in this process. In addition, OCC could be phosphorylated on tyrosine residues by src-like tyrosine kinase, c-Yes.[43] This phosphorylation site at the C terminus appeared to be critically important for its interaction with ZO-1, -2, and -3 molecules.[44]

Little information is available regarding the direct phosphorylation of CLD5 by known protein kinases. Endothelial cells exposed to cAMP demonstrated CLD5 phosphorylation at T207, in both protein kinase A (PKA)-dependent and -independent manners in porcine brain endothelial cells.[45,46] Soma and colleagues[45] admitted that its physiological significance in the endothelial cell TJ remained unclear. T207 is exactly the same site we found to be phosphorylated by RhoK in the present study. Overexpression of the T207A mutant but not wild-type CLD5 restored the barrier tightness and decreased permeability for mannitol (182 Da) in leaky lung endothelial cells.[45] Thus, CLD5 T207 phosphorylation could be critical for the BBB permeability for small molecules. We demonstrated before that migration of HIV-1-infected or uninfected monocytes caused diminished BBB integrity and phosphorylation of TJ proteins via activation of RhoA and RhoK, and inhibition of RhoA/RhoK in endothelial cells hampered monocyte migration, TJ phosphorylation, and barrier impairment during their migration across the monocyte barrier.[20] Our results suggest that RhoK can mediate PKA-independent phosphorylation of CLD5 at T207 during interactions with monocytes.

The OCC phosphorylation by RhoK was less efficient as compared to CLD5 and MLC. Although we observed endogenously phosphorylated OCC at T382 in COS-7 cells, the phosphorylation of recombinant OCC was only partially inhibited by the RhoK-specific inhibitor Y27632. These data suggest that although OCC is phosphorylated at T382, it is only partially regulated by RhoK, and other kinases mediate the phosphorylation. Thus, it will be of interest to characterize the OCC kinase that phosphorylates T382 using our specific anti-phospho T382 antibody.

The CLD5 phosphorylation by RhoK at T207 was corroborated by phosphopeptide mapping, radiolabeling,

and dot blot using anti-T207 antibody. T207 phosphorylation of full-length CLD5 was totally inhibited by Y27632 in COS-7 cells. These data strongly suggest that RhoK is one of CLD5 kinases. Thus, RhoK appears to be involved in BBB dysfunction through modification of TJs, because CLD5 is abundantly expressed in brain microvasculature, and its disruption by gene targeting results in BBB leakage.[13,47] The phosphorylation of T207 may interfere with its association with TJ anchoring molecules (such as ZOs) leading to CLD5 destabilization at plasma membrane. Further studies are necessary to characterize the altered CLD5 interactions with other TJ molecules on its phosphorylation. Importantly, phosphospecific antibodies detected phosphorylation of CLD5 and OCC in mouse endothelial cells because of RhoA/RhoK activation, and TJ phosphorylation paralleled decreased barrier tightness. Suppression of RhoK activity prevented these changes, suggesting that RhoK inhibitors could protect BBB. Tightness of the endothelial barrier as indicated by TEER readings (typically ~2600 Ω/cm^2) was higher than the reported TEER of human BMECs (1500 ~ 1800 Ω).[48] This may be attributable to the differences in experimental design (400 Hz reading instead of 4000 Hz) and readout of parameters (resistance instead of impedance). Indeed, Hartmann and colleagues[49] reported much higher TEER reading (15,000 Ω) from porcine BMECs using the same instrument (ECIS model 1600R) and readings (400 Hz) as ours.

Detection of phosphorylated CLD5 and OCC at cell borders of BMVECs in HIVE mouse brains provides direct evidence that chronic activation of RhoK phosphorylates TJ proteins paralleling BBB dysfunction. Detection of phosphorylated TJ proteins outside of mononuclear cell infiltration suggests that other factors (such as proinflammatory cytokines, chemokines, or viral proteins) present in the blood of HIVE animals could chronically disrupt BBB as indicated by *in vitro* results.[50] There is also spatial and temporal delay in OCC and CLD5 phosphorylation events and ligand stimulation or cell contact *in vivo*. Our current *in vitro* work further addresses the molecular mechanism of protein phosphorylation and barrier dysfunction under these conditions. Phosphospecific antibodies generated by us can be used for monitoring the chronic activation of TJ kinases, including RhoK, and the extent of BBB leakage *in vivo*. Suppression of RhoK via specific inhibitors or upstream Rho GTPases might be a potential treatment approach for BBB injury associated with neuroinflammation.

Acknowledgments

We thank Dr. Shoichiro Tsukita for mouse CLD5 and OCC cDNAs; Mrs. Robin Taylor and Mr. Michael Jacobsen for excellent manuscript editing.

References

1. Pardridge WM: Brain metabolism: a perspective from the blood-brain barrier. Physiol Rev 1983, 63:1481–1535
2. Morita K, Furuse M, Fujimoto K, Tsukita S: Claudin multigene family encoding four-transmembrane domain protein components of tight junction strands. Proc Natl Acad Sci USA 1999, 96:511–516
3. Hawkins BT, Davis TP: The blood-brain barrier/neurovascular unit in health and disease. Pharmacol Rev 2005, 57:173–185
4. Wolburg H, Lippoldt A: Tight junctions of the blood-brain barrier: development, composition and regulation. Vasc Pharmacol 2002, 38:323–337
5. Furuse M, Hirase T, Itoh M, Nagafuchi A, Yonemura S, Tsukita S: Occludin: a novel integral membrane protein localizing at tight junctions. J Cell Biol 1993, 123:1777–1788
6. Hirase T, Staddon JM, Saitou M, Ando-Akatsuka Y, Itoh M, Furuse M, Fujimoto K, Tsukita S, Rubin LL: Occludin as a possible determinant of tight junction permeability in endothelial cells. J Cell Sci 1997, 110:1603–1613
7. Vorbrodt AW, Dobrogowska DH: Molecular anatomy of intercellular junctions in brain endothelial and epithelial barriers: electron microscopist's view. Brain Res Brain Res Rev 2003, 42:221–242
8. Sakakibara A, Furuse M, Saitou M, Ando-Akatsuka Y, Tsukita S: Possible involvement of phosphorylation of occludin in tight junction formation. J Cell Biol 1997, 137:1393–1401
9. Hirase T, Kawashima S, Wong E, Uemada T, Rikitake Y, Tsukita S, Yokoyama M, Staddon J: Regulation of tight junction permeability and occludin phosphorylation by RhoA-p160ROCK-dependent and independent mechanism. J Biol Chem 2001, 276:10423–10431
10. Wachtel M, Frei K, Ehler E, Fontana A, Winterhalter K, Gloor SM: Occludin proteolysis and increased permeability in endothelial cells through tyrosine phosphatase inhibition. J Cell Sci 1999, 112: 4347–4356
11. Fanning AS, Jameson BJ, Jesaitis LA, Anderson JM: The tight junction protein ZO-1 establishes a link between the transmembrane protein occludin and the actin cytoskeleton. J Biol Chem 1998, 273:29745–29753
12. Furuse M, Hata M, Furuse K, Yoshida Y, Haratake A, Sugitani Y, Noda T, Kubo A, Tsukita S: Claudin-based tight junctions are crucial for the mammalian epidermal barrier: a lesson from claudin-1-deficient mice. J Cell Biol 2002, 156:1099–1111
13. Nitta T, Hata M, Gotoh S, Seo Y, Sasaki H, Hashimoto N, Furuse M, Tsukita S: Size-selective loosening of the blood-brain barrier in claudin-5-deficient mice. J Cell Biol 2003, 161:653–660
14. Morita K, Sasaki H, Furuse K, Furuse M, Tsukita S, Miyachi Y: Expression of claudin-5 in dermal vascular endothelia. Exp Dermatol 2003, 12:289–295
15. Kubota K, Furuse M, Sasaki H, Sonoda N, Fujita K, Nagafuchi A, Tsukita S: Ca(2+)-independent cell-adhesion activity of claudins, a family of integral membrane proteins localized at tight junctions. Curr Biol 1999, 9:1035–1038
16. Rolfe BE, Worth NF, World CJ, Campbell JH, Campbell GR: Rho and vascular disease. Atherosclerosis 2005, 183:1–16
17. Etienne S, Adamson P, Greenwood J, Strosberg AD, Cazaubon S, Couraud PO: ICAM-1 signaling pathways associated with Rho activation in microvascular brain endothelial cells. J Immunol 1998, 161:5755–5761
18. Etienne-Manneville S, Manneville JB, Adamson P, Wilbourn B, Greenwood J, Couraud PO: ICAM-1-coupled cytoskeletal rearrangements and transendothelial lymphocyte migration involve intracellular calcium signaling in brain endothelial cell lines. J Immunol 2000, 165:3375–3383
19. Van Wetering S, Van Den Berk N, Van Buul JD, Mul FP, Lommerse I, Mous R, Ten Klooster JP, Zwaginga JJ, Hordijk PL: VCAM-1-mediated Rac signaling controls endothelial cell-cell contacts and leukocyte transmigration. Am J Physiol Cell Physiol 2003, 285:C343–C352
20. Persidsky Y, Heilman D, Haorah J, Zelivyanskaya M, Persidsky R, Weber GA, Shimokawa H, Kaibuchi K, Ikezu T: Rho-mediated regulation of tight junctions during monocyte migration across the blood-brain barrier in HIV-1 encephalitis (HIVE). Blood 2006, 107: 4770–4780
21. Amano M, Mukai H, Ono Y, Chihara K, Matsui T, Hamajima Y, Okawa K, Iwamatsu A, Kaibuchi K: Identification of a putative target for Rho as the serine-threonine kinase protein kinase N. Science 1996, 271:648–650
22. Laemmli UK: Cleavage of structural proteins during the assembly of the head of bacteriophage T4. Nature 1970, 227:680–685
23. Kayser JP, Vallet JL, Cerny RL: Defining parameters for homology-tolerant database searching. J Biomol Tech 2004, 15:285–295

24. Brown RC, Morris AP, O'Neil RG: Tight junction protein expression and barrier properties of immortalized mouse brain microvessel endothelial cells. Brain Res 2007, 1130:17–30
25. Omidi Y, Campbell L, Barar J, Connell D, Akhtar S, Gumbleton M: Evaluation of the immortalised mouse brain capillary endothelial cell line, b.End3, as an in vitro blood-brain barrier model for drug uptake and transport studies. Brain Res 2003, 990:95–112
26. Gendelman HE, Orenstein JM, Martin MA, Ferrua C, Mitra R, Phipps T, Wahl LA, Lane HC, Fauci AS, Burke DS, Skillman D, Meltzer MS: Efficient isolation and propagation of human immunodeficiency virus on recombinant colony-stimulating factor 1-treated monocytes. J Exp Med 1988, 167: 1428–1441
27. Persidsky Y, Limoges J, McComb R, Bock P, Baldwin T, Tyor W, Patil A, Nottet HS, Epstein L, Gelbard H, Flanagan E, Reinhard J, Pirruccello SJ, Gendelman HE: Human immunodeficiency virus encephalitis in SCID mice. Am J Pathol 1996, 149:1027–1053
28. Potula R, Poluektova L, Knipe B, Chrastil J, Heilman D, Dou H, Takikawa O, Munn DH, Gendelman HE, Persidsky Y: Inhibition of indoleamine 2,3-dioxygenase (IDO) enhances elimination of virus-infected macrophages in an animal model of HIV-1 encephalitis. Blood 2005, 106:2382–2390
29. Potula R, Haorah J, Knipe B, Leibhart J, Chrastil J, Heilman D, Dou H, Reddy R, Ghorpade A, Persidsky Y: Alcohol abuse enhances neuroinflammation and impairs immune responses in an animal model of human immunodeficiency virus-1 encephalitis. Am J Pathol 2006, 168:1335–1344
30. Zink WE, Anderson E, Boyle J, Hock L, Rodriguez-Sierra J, Xiong H, Gendelman HE, Persidsky Y: Impaired spatial cognition and synaptic potentiation in a murine model of human immunodeficiency virus type 1 encephalitis. J Neurosci 2002, 22:2096–2105
31. Kimura K, Ito M, Amano M, Chihara K, Fukata Y, Nakafuku M, Yamamori B, Feng J, Nakano T, Okawa K, Iwamatsu A, Kaibuchi K: Regulation of myosin phosphatase by Rho and Rho-associated kinase (Rho-kinase). Science 1996, 273:245–248
32. Sato S, Cerny RL, Buescher JL, Ikezu T: Tau-tubulin kinase 1 (TTBK1), a neuron-specific tau kinase candidate, is involved in tau phosphorylation and aggregation. J Neurochem 2006, 98:1573–1584
33. Koto T, Takubo K, Ishida S, Shinoda H, Inoue M, Tsubota K, Okada Y, Ikeda E: Hypoxia disrupts the barrier function of neural blood vessels through changes in the expression of claudin-5 in endothelial cells. Am J Pathol 2007, 170:1389–1397
34. Song L, Pachter JS: Culture of murine brain microvascular endothelial cells that maintain expression and cytoskeletal association of tight junction-associated proteins. In Vitro Cell Dev Biol Anim 2003, 39: 313–320
35. van Nieuw Amerongen GP, Vermeer MA, van Hinsbergh VW: Role of RhoA and Rho kinase in lysophosphatidic acid-induced endothelial barrier dysfunction. Arterioscler Thromb Vasc Biol 2000, 20: E127–E133
36. Poluektova LY, Munn DH, Persidsky Y, Gendelman HE: Generation of cytotoxic T cells against virus-infected human brain macrophages in a murine model of HIV-1 encephalitis. J Immunol 2002, 168: 3941–3949
37. Zink WE, Zheng J, Persidsky Y, Poluektova L, Gendelman HE: The neuropathogenesis of HIV-1 infection. FEMS Immunol Med Microbiol 1999, 26:233–241
38. Persidsky Y, Poluektova L: Immune privilege and HIV-1 persistence in the CNS. Immunol Rev 2006, 213:180–194
39. Antonetti DA, Barber AJ, Hollinger LA, Wolpert EB, Gardner TW: Vascular endothelial growth factor induces rapid phosphorylation of tight junction proteins occludin and zonula occluden 1. A potential mechanism for vascular permeability in diabetic retinopathy and tumors. J Biol Chem 1999, 274:23463–23467
40. Andreeva AY, Krause E, Muller EC, Blasig IE, Utepbergenov DI: Protein kinase C regulates the phosphorylation and cellular localization of occludin. J Biol Chem 2001, 276:38480–38486
41. Cordenonsi M, Turco F, D'Atri F, Hammar E, Martinucci G, Meggio F, Citi S: Xenopus laevis occludin. Identification of in vitro phosphorylation sites by protein kinase CK2 and association with cingulin. Eur J Biochem 1999, 264:374–384
42. Smales C, Ellis M, Baumber R, Hussain N, Desmond H, Staddon JM: Occludin phosphorylation: identification of an occludin kinase in brain and cell extracts as CK2. FEBS Lett 2003, 545:161–166
43. Chen YH, Lu Q, Goodenough DA, Jeansonne B: Nonreceptor tyrosine kinase c-Yes interacts with occludin during tight junction formation in canine kidney epithelial cells. Mol Biol Cell 2002, 13:1227–1237
44. Kale G, Naren AP, Sheth P, Rao RK: Tyrosine phosphorylation of occludin attenuates its interactions with ZO-1, ZO-2, and ZO-3. Biochem Biophys Res Commun 2003, 302:324–329
45. Soma T, Chiba H, Kato-Mori Y, Wada T, Yamashita T, Kojima T, Sawada N: Thr(207) of claudin-5 is involved in size-selective loosening of the endothelial barrier by cyclic AMP. Exp Cell Res 2004, 300:202–212
46. Ishizaki T, Chiba H, Kojima T, Fujibe M, Soma T, Miyajima H, Nagasawa K, Wada I, Sawada N: Cyclic AMP induces phosphorylation of claudin-5 immunoprecipitates and expression of claudin-5 gene in blood-brain-barrier endothelial cells via protein kinase A-dependent and -independent pathways. Exp Cell Res 2003, 290:275–288
47. Ohtsuki S, Sato S, Yamaguchi H, Kamoi M, Asashima T, Terasaki T: Exogenous expression of claudin-5 induces barrier properties in cultured rat brain capillary endothelial cells. J Cell Physiol 2007, 210:81–86
48. Chang YC, Stins MF, McCaffery MJ, Miller GF, Pare DR, Dam T, Paul-Satyaseela M, Kim KS, Kwon-Chung KJ: Cryptococcal yeast cells invade the central nervous system via transcellular penetration of the blood-brain barrier. Infect Immun 2004, 72:4985–4995
49. Hartmann C, Zozulya A, Wegener J, Galla HJ: The impact of glia-derived extracellular matrices on the barrier function of cerebral endothelial cells: an in vitro study. Exp Cell Res 2007, 313:1318–1325
50. Kanmogne GD, Schall K, Leibhart J, Knipe B, Gendelman HE, Persidsky Y: HIV-1 gp120 compromises blood-brain barrier integrity and enhances monocyte migration across blood-brain barrier: implication for viral neuropathogenesis. J Cereb Blood Flow Metab 2007, 27:123–134